Characterization of flow direction in microchannels and zebrafish blood vessels by scanning fluorescence correlation spectroscopy

Citation: Pan, Xiaotao, Hanry Yu, Xianke Shi, Vladimir Korzh, and Thorsten Wohland. "Characterization of Flow Direction in Microchannels and Zebrafish Blood Vessels by Scanning Fluorescence Correlation Spectroscopy." Journal of Biomedical Optics 12, no. 1 (2007): 014034.

As Published: http://dx.doi.org/10.1117/1.2435173

Publisher: SPIE

Persistent URL: http://hdl.handle.net/1721.1/87647

Version: Final published version: final published article, as it appeared in a journal, conference proceedings, or other formally published context

Characterization of flow direction in microchannels and zebrafish blood vessels by scanning fluorescence correlation spectroscopy

Xiaotao Pan
National University of Singapore
NUS Graduate Program in Bioengineering
28 Medical Drive
Singapore 117456 Singapore
and
National University of Singapore
Department of Chemistry
3 Science Drive 3
Singapore 117543 Singapore

Hanry Yu
National University of Singapore
NUS Graduate Program in Bioengineering
28 Medical Drive
Singapore 117456 Singapore
and
National University of Singapore
Department of Physiology and NUSTEP
2 Medical Drive
Singapore 117597 Singapore
and
Institute of Bioengineering and Nanotechnology
A*STAR, 31 Biopolis Way
The Nanos #04-01
Singapore 138669, Singapore
and
Singapore-MIT Alliance
E4-04-10, 4 Engineering Drive 3
Singapore 117576 Singapore

Xianke Shi
National University of Singapore
Department of Chemistry
3 Science Drive 3
Singapore 117543 Singapore

Vladimir Korzh
Institute of Molecular and Cell Biology
61 Biopolis Drive, Proteos
Singapore 138673 Singapore

Thorsten Wohland
National University of Singapore
NUS Graduate Program in Bioengineering
28 Medical Drive
Singapore 117456 Singapore
and
National University of Singapore
Department of Chemistry
3 Science Drive 3
Singapore 117543 Singapore
E-mail: chmwt@nus.edu.sg

Abstract. The investigation of flow profiles in microstructures and tissues by fluorescence correlation spectroscopy (FCS) has been a challenging topic in the past decade. Due to its inherent optical configuration, a circular focused laser beam, FCS is unable to resolve microfluidic flow directions. Earlier schemes reported the use of two laser beams or the use of nonsymmetrical laser foci to break the symmetry of the measurement system. This, however, is difficult to combine with confocal systems since it would require modifications that interfere with the imaging capabilities. We propose a method called line-scan FCS to measure different flow angles in microchannels and tissues. This method is implemented on a combined laser scanning confocal microscopy (LSCM) and FCS system that enables uncompromised imaging and spectroscopy measurements. We demonstrate that by scanning the laser beam with a defined speed and direction we can measure flow direction with the current system at an optimal resolution of at least 3 μm. The combination system is assessed by measuring flow profiles in a microchannel with and without obstruction. To extend the technique to live tissue measurements we demonstrate that line-scan FCS can determine the flow direction in zebrafish small blood vessels in a label-free approach. [DOI: 10.1117/1.2435173]

Keywords: fluorescence correlation spectroscopy; scanning fluorescence correlation spectroscopy; microchannel; flow profile; zebrafish.

Paper 06113R received May 3, 2006; revised manuscript received Oct. 31, 2006; accepted for publication Nov. 11, 2006; published online Feb. 2, 2007.

1 Introduction

Great attention has been paid in the past decade to flow velocity measurements in microscale miniaturized structures in the fields of chemical analysis and biological sciences. Development of microfabrication technologies for lab-on-a-chip devices has enabled the application of microfluidic systems in drug testing,[1] sorting of cells,[2] DNA characterization,[3] polymerase chain reactions,[4] and biochemical analyses. Currently, microchannels incorporating microfluidics have been reported to assist *in vitro* cell culture in tissue engineering.[5–7] It is necessary to understand the flow patterns in these microchips to help engineers to improve the performance of fluidic systems as well as to enable the evaluation of mass-transport-limited reaction patterns. Another important subject is the measurement of flow profiles in living tissues and organisms. The investigation of blood flow *in vivo* can provide information about the environment of endothelial cells,[8–10] a precondition for mimicking and optimizing the physiological conditions in culture systems. Various approaches have been proposed and applied to monitor the fluid flow in microscale systems and even animal bodies in the past decade including particle image velocimetry[11] (PIV), laser speckle imaging,[12]

Address all correspondence to Thorsten Wohland, Chemistry, National University of Singapore, 3 Science Drive 3, Singapore, Singapore 117543 Singapore; Tel: +65 65161248; Fax: +65 67791691; E-mail: chmwt@nus.edu.sg

1083-3668/2007/12(1)/014034/10/$25.00 © 2007 SPIE

optical Doppler tomography,[13] nuclear magnetic resonance (NMR) imaging.[14] However, most of them are limited either in spatial resolution or in high concentration of larger probes. For example, PIV requires the use of a sufficient number of microbeads, which might cause severe obstruction of flow and distortion of the flow profile in these micrometer sized structures.

An alternative for microfluid flow measurements is fluorescence correlation spectroscopy (FCS), which measures the time fluorescent molecules require to pass through a confocal observation volume.[15,16] FCS can work at very low concentrations of small fluorescent molecules with high spatial resolution, circumventing the problems of PIV. Its experimental validation particularly in flow was demonstrated in the transport of large protein units in plant cells,[17] enhanced yellow fluorescent protein (EYFP) bacteria flowing in a capillary,[18] and DNA molecules in a microfluidic channel[3] but not in living tissues. In addition to single-point measurements, FCS has been extended to obtain flow profiles by positioning the observation volume point by point in a microfluidic channel,[19] so as to acquire microfluid velocity images vertically and horizontally.[20] However, the FCS probe volume is rotationally symmetric in the focal plane, thus no information about flow directions can be obtained. A rectangular or elliptical laser beam cross section was used, thus breaking the symmetry of the probe volume in the plane of focus.[21] In these systems, the traveling time of molecules through the observation volume depends on the structural extension of the focal volume in flow direction and varies from a minimum, when the flow is parallel to the short axis, to a maximum, when the flow is along the long axis. However, the methods measure only different flowing times but not flow velocities because of the focal volume geometry, while the flow direction is still ambiguous since opposite flows cannot be distinguished. Their applications in biological tissues are limited for these strategies because the focal geometry can not be accurately characterized due to the refractive index distortion in biological specimens. The other improved schemes are dual-beam FCS (Ref. 22), coupled with techniques of two-color cross-correlation[23] and time-delayed two-photon pulse excitation.[24] But their drawbacks are low spatial resolution for directionality analysis and limited detection efficiency at large flow angles. No application of these two methods in practical systems for actual angle determination has been presented so far.

Scanning FCS since its invention has been used for various biological applications.[25,26] Additionally, two-photon excitation improves its detection efficiency and accuracy.[27] Recently, two kinds of scanning FCS techniques are reported to measure protein or molecule flow velocity, such as spatiotemporal image correlation spectroscopy[28] (STICS) and circular scan FCS (so-called PSFCS; Ref. 29). In this paper, line-scan FCS is proposed for the analysis of flow profiles in microchannels and even living tissues. Here we present a modified laser scanning confocal microscope (LSCM) that enables FCS measurements and performs line-scan FCS as one of its functions. Under defined conditions, the line scans can be considered as quasisingle directional for FCS analysis. Hence, by linearly scanning the probe volume through the sample one introduces an external single directional "flow" into the microfluidic system without internal disruption. If the speeds of internal microfluid flow, external "flow" and the net flow are measured, the angles formed by external flow and internal microfluid flow can be calculated. Importantly, line-scan FCS has the advantage that the scanning speed is the key parameter to resolve flow directions, which is critical for the cases such as tissue measurements when the focus geometry is unknown. This method is verified by the investigations of flow profiles in a center-obstructed microchannel and applied to the determination of blood flow angles in small vessels in an immobilized living zebrafish embryo.

2 Theory

2.1 *FCS Measurements*

FCS measures temporal intensity fluctuations of fluorescent molecules caused by their dynamic processes, such as diffusion or flow, within a small open volume that is defined by a focused laser beam. The autocorrelation function (ACF) of the fluorescence fluctuation signal for pure 3-D diffusion is given by[15,30,31]

$$G(\tau)=\left[\frac{F_{\mathrm{trip}}}{1-F_{\mathrm{trip}}}\exp\left(-\frac{\tau}{\tau_{\mathrm{trip}}}\right)+1\right]\frac{1}{N}\left(1+\frac{\tau}{\tau_d}\right)^{-1}\times\left(1+\frac{\tau}{K^2\tau_d}\right)^{-1/2}+G_\infty, \quad (1)$$

where N is the number of molecules; τ_d is the diffusion time of molecules through the focal volume; τ_{trip} is the relaxation time of the molecule from the triplet state to the ground state; F_{trip} is the fraction of the number of molecules in the triplet state; the structural parameter K is defined as z_0/ω_0, an important factor to characterize the optical alignment; and ω_0 and z_0 are its radial and axial extensions, defined as the distance from the focal point where the intensity has decreased by a factor of e^{-2} compared to the central intensity.

2.2 *FCS Flow Analysis*

Measurement of microfluid flow speeds by FCS was first described with the assumption that flow is uniform and single-directional in a plane perpendicular to the optical axis. The normalized ACF in the case for a single flow component coupled with free diffusion results in a one-flow model is[16,22]

$$G_1(\tau)=\left[\frac{F_{\mathrm{trip}}}{1-F_{\mathrm{trip}}}\exp\left(-\frac{\tau}{\tau_{\mathrm{trip}}}\right)+1\right]\frac{1}{N}g(\tau)\times\exp\left[-\left(\frac{\tau}{\tau_f}\right)^2\left(1+\frac{\tau}{\tau_d}\right)^{-1}\right]+G_\infty,$$
$$\text{with}\quad g(\tau)=\left(1+\frac{\tau}{\tau_d}\right)^{-1}\left(1+\frac{\tau}{K^2\tau_d}\right)^{-1/2}, \quad (2)$$

where τ_f is the traveling time of molecules through the focal volume. The flow speed is calculated as $V=\omega_0/\tau_f$. Note that a single directional scan of the laser focus with constant velocity in a static solution will generate the same flow pattern[25] [Eq. (2)].

2.3 *Laser Focus Bidirectional Scans*

When two independent flow components are present in FCS measurements, the ACF can be expressed as a two-flow model

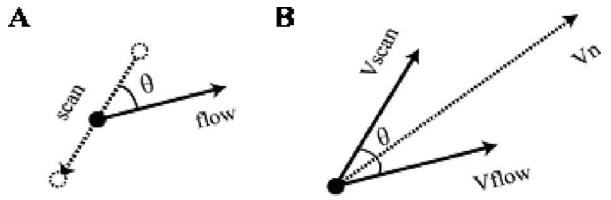

Fig. 1 (A) Single-point FCS implemented at the black spot, line-scan FCS performed along the dashed line, and the direction of microfluidic flow (V_{flow}) indicated by an arrow; and (B) schematic relationship of the laser beam scan (V_{scan}) and the net velocity (V_n), taking the laser focal spot as a reference point.

[Eq. (3)]. This situation usually arises only when the two flow components exist independently at different times, as is the case in an organism with a heart beat, where systolic and diastolic flow is different, or any system in which the flow is alternated between two different flows. This is also the case when, e.g., using bidirectional scans of a laser scanning confocal microscope with alternating forward and backward scans of different speeds. Under the assumption that the scan times are larger than the diffusion time ($T_{\text{forward}} > \tau_d$, $T_{\text{backward}} > \tau_d$), the forward and backward scans can be treated as independent. Therefore, the resulting ACF for laser bidirectional scans is represented by a two-flow model:

$$G_2(\tau) = \left[\frac{F_{\text{trip}}}{1-F_{\text{trip}}}\exp\left(-\frac{\tau}{\tau_{\text{trip}}}\right)+1\right]\frac{1}{N}g(\tau) \times\left\{F_{f_1}\exp\left[-\left(\frac{\tau}{\tau_{f_1}}\right)^2\left(1+\frac{\tau}{\tau_d}\right)^{-1}\right]+(1-F_{f_1}) \times\exp\left[-\left(\frac{\tau}{\tau_{f_2}}\right)^2\left(1+\frac{\tau}{\tau_d}\right)^{-1}\right]\right\}+G_\infty, \quad (3)$$

where F_{f_1} is the fraction of time the system experiences the flow with a characteristic flow time τ_{f_1}, and $1-F_{f_1}$ is the fraction of time the system experiences the flow with a characteristic flow time τ_{f_2}. For the case of the bidirectional scans, $F_{f_1}=T_{\text{forward}}/(T_{\text{forward}}+T_{\text{backward}})$, where T_{forward} and T_{backward} represent the times during which the system experiences forward and backward scans.

2.4 *Analysis of Flow Directions*

As illustrated in Fig. 1(A), the laser beam is scanned at an angle of θ with respect to the flow direction in the microchannel. By considering the scanning laser focus as a reference, and assuming a constant scan speed in one direction, a schematic diagram of relative velocities can be drawn [Fig. 1(B)], where V_n is the net velocity vector of the combined flows of V_{scan} and V_{flow}. The mathematical relationship of those three velocities can be defined by the equation as follows:

$$V_n^2 = V_{\text{scan}}^2 + V_{\text{flow}}^2 - (2V_{\text{scan}})(V_{\text{flow}})[\cos(180-\theta)]. \quad (4)$$

Note that V_{scan} can be determined for a specific instrument by single-point FCS flow analysis in a solution without flow, V_{flow} can be measured in the flowing sample solution with a stationary laser focus, and V_n is measured in the same flowing sample while linearly scanning the laser focus. With these three parameters known, the angle θ can be calculated.

$$\theta = 180 - \cos^{-1}\left[\frac{V_{\text{scan}}^2 + V_{\text{flow}}^2 - V_n^2}{(2V_{\text{scan}})(V_{\text{flow}})}\right]. \quad (5)$$

As long as the laser line scan direction is known, the flow angle can be determined as $\theta_{\text{flow}}=\theta_{\text{scan}}-\theta$. This is true under the assumption that flow speed and direction in the sample does not vary significantly over the scanning distance. Therefore, the resolution of this method is limited by the length of the scan line.

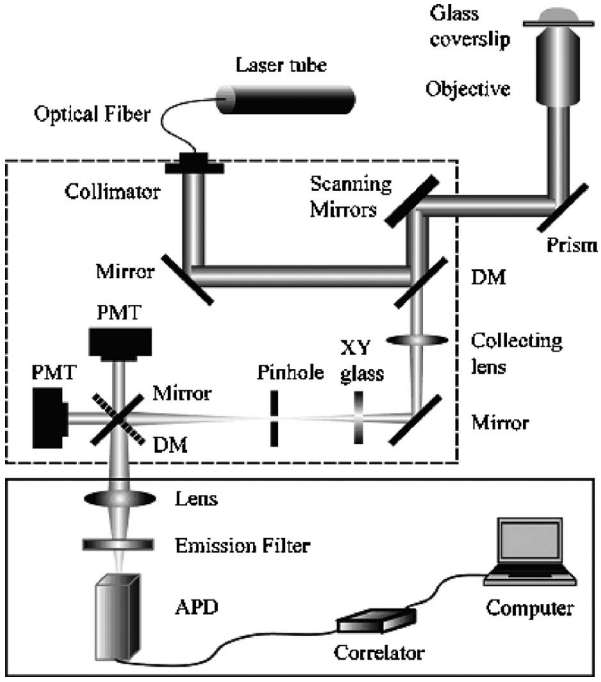

Fig. 2 Schematic diagram of a combination optical system of LSCM and FCS: DM, dichroic mirror; PMT, photomultiplier tube; APD, avalanche photodiodes.

3 Experimental

3.1 *Optical System Setup*

A commercial LSCM (FV300, Olympus, Singapore) was modified and combined with FCS. For the FV300, a HeNe laser (543 nm, Melles Griot, Singapore) is coupled into the scanning unit (Fig. 2, dashed box) after passing through an optical fiber, and reflected by a mirror and an excitation dichroic mirror (488/543/633) into a pair of galvanometer scanning mirrors (G120DT, GSI Lumonics). After being scanned, the laser beam is directed into a water immersion objective [60×, numerical aperture (NA) 1.2, Olympus, Singapore] by a reflective prism and focused into a small focal volume in the specimen. The fluorescence emitted from the sample is collected by the same objective, descanned, and focused again by a collecting lens into a confocal pinhole. A glass slab is used for light beam *xy* position alignment. A modified detection part (Fig. 2, solid box) for FCS was mounted on the top of the scanning unit. The fluorescence light after the confocal pinhole is imaged by a lens (Achromats $f=60$ mm, Linos, Goettingen, Germany), through an emission filter (580DF30,

Omega, Brattleboro, Vermont, USA), into the active area of an avalanche photodiode (APD) in a single-photon-counting module (SPCM-AQR-14, Pacer Components, Berkshire, UK). The transistor-to-transistor logic (TTL) output signal from the APD is processed online by an autocorrelator (Flex02-01D, correlator.com, Zhejiang, China) to get an experimental ACF curve. Curve fitting is performed by a self-written program in Igor Pro (WaveMetrics, Lake Oswego, Oregon, USA).

3.2 *Selective Scan Length*

The analog voltage, a saw tooth signal used to control the scanner to perform the line scan, was acquired and converted to a digital signal (DAQCard 1200, National Instruments Singapore). A self-written program (LabView, National Instruments Singapore) was used to create a TTL output pulse for each minima of the saw tooth signal to synchronize the data acquisition with the line scan. The arrival times of these TTL pulses marking the start of a scan line and the signals from the APD were simultaneously recorded by a counter/timer device (PCI-6602, National Instruments Singapore). The synchronization of the fluorescence signal with the scanner enables the accurate selection of data acquired during any specific phase of the line scan. The ACF data calculation and curve fitting were completed by programming in Igor Pro.

3.3 *Microchannels*

Teflon is used to fabricate a microchannel mold with one inlet [Fig. 3(A), point a] and two outlets [Fig. 3(A), points b and c], its cross section is a rectangle of 380 μm width and 300 μm height. Prepolymer of polydimethylsiloxane (PDMS) (Sylgard 184, Dow-Corning, Midland, Michigan, USA) is poured over the molds and cured at 65°C overnight before peeling off. The PDMS membrane is oxidized in oxygen plasma for 1 min to be chemically bonded to a glass coverslip. To generate an obstruction flow pattern, a fiber with a radius of 100 μm is inserted into the center of a microchannel after the fabrication process [Fig. 3(A), point d]. A syringe pump (KDS100, Fisher Scientific, Singapore) is employed for the perfusion of probe solution into the microchannels through tubing and connectors. Different flow velocities in the microchannel can be induced by varying the syringe pump rates.

3.4 *Zebrafish*

The maintenance of zebrafish was based on the protocols in the zebrafish book.[32] Briefly, a pair of AB wild-type zebrafish was crossed and their embryos were collected the next morning. The embryos were then incubated in egg water [60 μg/ml, Instant Ocean® sea salts (Aquarium Systems, Inc.)] at 28.5°C for the optimal development, and after 20 hpf (hours postfertilization) PTU (0.003% 1-phenyl-2-thiourea in 10% Hank's saline, Invitrogen, Singapore) was added to prevent pigmentation. Embryos were dechorionated at the time of 55 h and then anaesthetized by Tricaine (ethyl m-aminoboenzoate, Sigma, Singapore). The treated embryos were mounted in 0.5% low-melting-temperature agarose (Invitrogen, Singapore) in a WillCo-dish® glass bottom dish (GW-3512, WillCo-Wells, The Netherlands) for the following measurements.

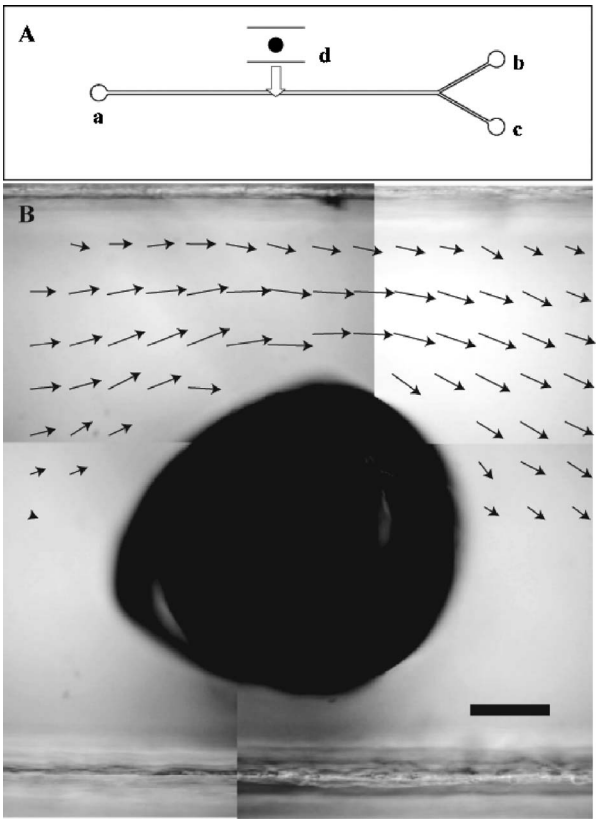

Fig. 3 (A) PDMS-glass microchannel structure that has an inlet (point a) and two outlets (points b and c). An obstruction flow pattern is achieved by a fiber inserted in the center of the microchannel, as shown in the inset (point d). (B) Flow velocity vectors measured by line-scan FCS plotted around an obstacle fiber in the microchannel. The length and arrow of those vectors represent the flow speed and direction (bar, 50 μm).

3.5 *Procedures*

A dye solution (1 nM, atto565, Sigma, Singapore) was prepared in deionized water as a probe for all flow measurements. Excitation was at a power of ~100 μW just before the objective provided by a HeNe laser (543 nm). Line-scan speeds of different scan modes, such as fast, medium, and slow, were calibrated and measured in a static dye solution; various flow speeds induced by a syringe pump were obtained by single-point FCS measurements and the combined speeds of flow and scan were acquired by line-scan FCS. As a compromise of the accuracy and resolution, a slow scan line of 3 μm, perpendicular to the channel wall, was selected for the applications of the method in flow velocity mapping in microchannels and zebrafish tissues. The acquisition time was 30 s for all measurements. The structural parameter K, extracted from a calibration measurement, was the only parameter to be fixed for the following data fitting.

4 Results and Discussion

4.1 *Optical Calibrations*

To characterize the combination system, a probe solution of atto565 (1 nM) was sealed in a rubber-glass chamber and ACF curves at 9×9 points were acquired by single-point

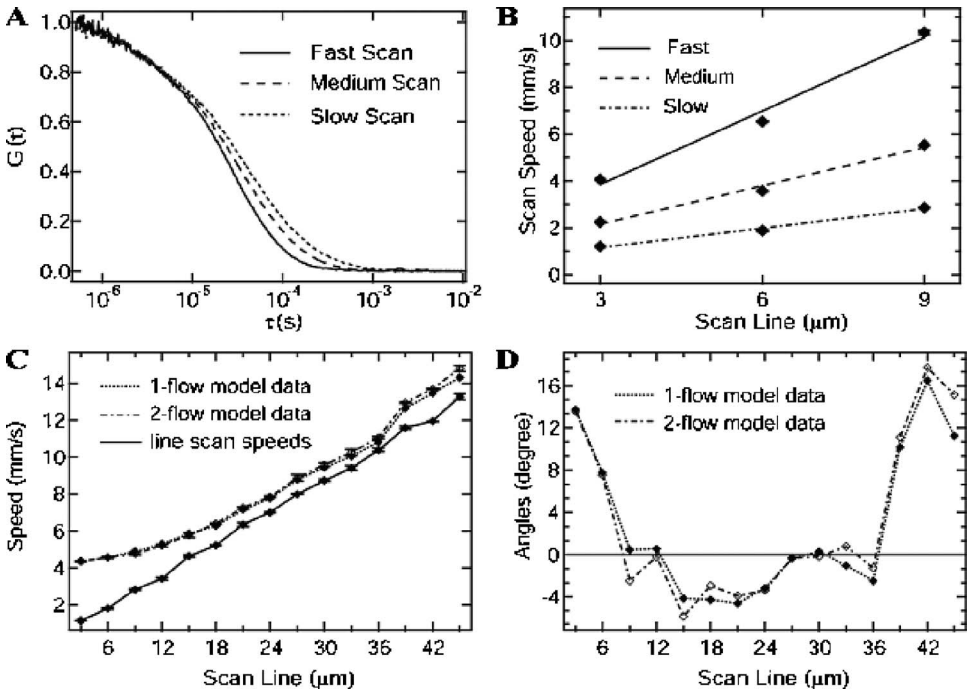

Fig. 4 (A) Three normalized ACF curves for a 3-μm line scan in different scan modes; (B) the average line-scan speeds of different lengths, such as 3, 6, and 9 μm, at different scan modes analyzed by the one-flow model; (C) forward line-scan speeds obtained by the two-flow model and the net speeds by both the one-flow and the two-flow fit models; and (D) flow angles calculated by these three speeds demonstrated with respect to the different lengths of scan lines.

FCS measurements. From the obtained contour figures of τ_d and K (data not shown), the aberrations are found not to significantly affect the values of τ_d and K in a circular area with a radius of 75 μm, about 2/3 of the full field of view. The central point value of τ_d was 45.10±0.17 μs, and the error for any measurement does not exceed 3.5%. The radial extension ω_0 at the central point can be calculated as $\omega_0=(4D\tau_d)^{1/2}=0.22$ μm, where D_{atto565} is calculated as 2.591×10^{-10} m^2 s^{-1}, assuming that the diffusion coefficient of rhodamine 6G is 2.8×10^{-10} m^2 s^{-1} [Ref. 30] and $D_{\text{atto565}}=D_{\text{Rho6G}}(M_{\text{Rho6G}}/M_{\text{atto565}})^{1/3}$ ($M_{\text{atto565}}=612.06$ g/mol). The implication of this fact is that the focal volume defined by the laser beam does not vary greatly at different positions in a central area of 150 μm diameter.

4.2 *Fit Models and Line Scans*

The confocal microscope FV300 has three bidirectional line-scan modes, namely, fast, medium, and slow. Time durations of these scan modes for one cycle ($T_{\text{forward}}+T_{\text{backward}}$) are 1.00+0.50, 1.80+0.55, and 3.20+0.60 ms, respectively, regardless of the lengths of the scan line, as determined from the scanning mirror voltages input by an oscilloscope. Three normalized ACF curves of 3-μm line scans in the modes of fast, medium, and slow are shown in Fig. 4(A). The shorter the scanning time, the faster will be the scan speeds, which is emphasized by a shorter decaying time in the ACF curve [τ_f, Eq. (2)]. Furthermore, the speed of a line scan is proportional to its length. The longer the line, the faster is the laser beam scan [Fig. 4(B)]. We use both a one-flow model [Eq. (2)] and a two-flow model [Eq. (3)] to fit the data, and fitting results are shown in Table 1. From the values of χ_ν^2, which is a good indicator of difference between the fitting functions and raw data,[33,34] we can see that for the medium and fast bidirectional line-scan modes, the fits tend to deviate more from the data. This is probably due to nonlinear behavior of the scan mirrors at the endpoints of the scan. Nevertheless, in all cases, the ratios of τ_{f_1} and τ_{f_2} are in good agreement with those of T_{forward} and T_{backward} for fast, medium, and slow scan modes as measured by the oscilloscope (Table 1, parentheses). Therefore, the scan speeds of forward (τ_{f_1}) and backward (τ_{f_2}) scans can be extracted by the two-flow fit model. To test which model is appropriate for a certain scan mode we calculated the level of significance that the two-flow model represents an actual improvement over the one-flow model by an F test.[35] For the fitting results shown in Table 1, the number of all data points is 550, and there are six free parameters for the one-flow fit model [Eq. (2)] and eight free parameters for the two-flow model [Eq. (3)] because the structural parameter K was fixed in the fitting. The P values from the F test are calculated as 93.4% for fast, 74.9% for medium, and 81.1% for slow scan modes. The fact that the P value is larger than 90% indicates that the two-flow fit model is applicable for the fast scans. For the medium and slow scans, the results show that the necessity of introducing the two-flow model is much less significant, and the one-flow model is acceptable for data fitting. This is probably due to their relatively large time ratios of forward scans over backward scans. In theory, the two-flow model can be simplified into a one-flow model only if $\tau_{f_1}\gg\tau_{f_2}$, since for this case, the temporal intensity fluctuations are mostly caused by τ_{f_1}, i.e., by the forward scan.

Table 1 Key parameters obtained by fitting ACF curves of fast, medium, and slow line scan modes with a one-flow and a two-flow model; for the ratio of τ_{f_1} over τ_{f_2}, values in parenthesis were measured by oscilloscope.

Modes	τ_f or τ_{f_1} (μs)	τ_{f_2} (μs)	τ_{f_1}/τ_{f_2}	F_{f_1}	χ^2	*F* Test
Fast	51.9±0.2				3.13±0.17	93.4%
	59.8±1.1	25.0	2.39 (2.00)	0.81±0.03	2.75±0.17	
Medium	92.1±0.9				1.25±0.16	74.9%
	97.2±2.4	26.9±3.2	3.61 (3.27)	0.92±0.05	1.18±0.12	
Slow	16.2±0.3				0.96±0.11	81.1%
	16.8±0.7	32.6±5.6	5.15 (5.33)	0.92±0.03	0.89±0.11	

As an experimental verification, the Atto 565 1-nM solution was perfused into the microchannel at a pumping rate of 0.8 ml/h, and the direction of the microchannel was manually adjusted to 0 deg. Slow scan lines perpendicular to the flow axis with different lengths from 3 to 45 μm with and without flow were used to measure the net speeds and the scan speeds [Fig. 4(C)]. Flow angles determined by the one-flow and the two-flow models are plotted against the scan lengths [Fig. 4(D)]. From the graph, the net speeds obtained by the two-flow model are almost the same as those from the one-flow model, and the results of flow angles by the two fit models overlap without great differences. This agrees with our previous assumption that the one-flow model is suitable for the scans in medium or slow modes. Therefore, in the following we assume to have only one scan speed for the slow line scans. Furthermore, as flow speeds differ greatly across the microchannel for a large distance, long scan lines (e.g., above 36 μm) yield large measurement errors. Short line scans may be influenced by the nonlinear behavior of the scan mirrors at the endpoints of a scan when the mirror changes scan directions, and the measured flow angles are affected. Lines from 9 to 36 μm resolve the flow directions best. The spatial resolution is important for the characterization of the flow velocity profile in a micrometer-size structure by line-scan FCS. However, the accuracy of angle determination is deteriorating as the length of scan line decreases [Fig. 4(D)]. As a compromise, we choose a scan line of 3 μm for the optimal resolution and reasonable accuracy of flow profile measurements.

4.3 *Flow Direction Analysis*

For the optimization of line-scan FCS, we investigated the influence of relative angles between microfluid flow directions and scan lines on the accuracy of analysis. However, it is demanding in practice to change the flow directions precisely in the microchannel for the current system. Alternatively, rotation of scan lines can be set through the FV300 software provided by Olympus. Slow line scans at 16 different angles between 0 and 360 deg are executed when the dye solution is stationary in the microchannel or flowing. Corresponding results of laser beam line scan speeds [Fig. 5(A)] and net speeds [Fig. 5(B)] are shown in polar graphs, where the length of scan line 1 is 3 μm, line 2 is 6 μm, line 3 is 12 μm, and line 4 is 25 μm. The standard deviation of flow directions determined by the four scan lines with different lengths in dependence of rotational angle is shown in Fig. 5(C). An example of the ACF curves of the laser line scan, microfluidic flow without scanning, and microfluidic flow with line scan are shown in Fig. 5(D) and the goodness of the fits are confirmed by the residuals. In all measurements, the standard deviation is large when the scan line is parallel to the flow axis, while it is relatively small in the range of scanning directions perpendicular to the flow axis.

4.4 *Scan Length Reduction*

In the current setup without access to the control of the scan mirrors, it is possible to acquire selected parts of the fluorescence signal during forward scans, as described in Sec. 3.2. The lengths of scan lines were then effectively reduced from 3 to 1.5, 1, and 0.5 μm, and the respective ACF curves are shown in Fig. 6. From the data fitting, the scan speed of the 3-μm line scan was 0.98±0.07 mm/s, while that of the 1.5-μm line scan was 1.22±0.03 mm/s, the 1-μm line scan was 1.39±0.16 mm/s, and the 0.5-μm line scan was 1.45±0.15 mm/s. The scan speed of the bidirectional line scan of 3 μm was slower than that of single directional line scan of 1.5 μm, which is due to the nonlinear scan effect at line endpoints in forward scans and also the small time fraction of backward scans for the line of 3 μm. The selection of signals from the central part of the forward scan reduces the influence of nonlinear effects at the endpoints of the scan, removes the backward scan contribution, and reduces the scan line and thus increases the spatial resolution of the technique. However, the signal selection also reduces the measurement time and thus the signal collection since signals are recorded only during a fraction of the total scan.

4.5 *Applications*

To examine the applications in different systems, slow line scans of 3 μm were performed to determine the microfluidic flow directions. We investigated a microchannel with a fiber obstructed in the center [Fig. 3(A), point d] and measured its flow velocity pattern. In the microchannel, flow around the fiber is constricted to the horizontal plane, which implies the formation of a 2-D flow pattern inside. Line-scan FCS measurements are performed at 7×14 positions surrounding the fiber with a step size of 30 μm for the determination of the

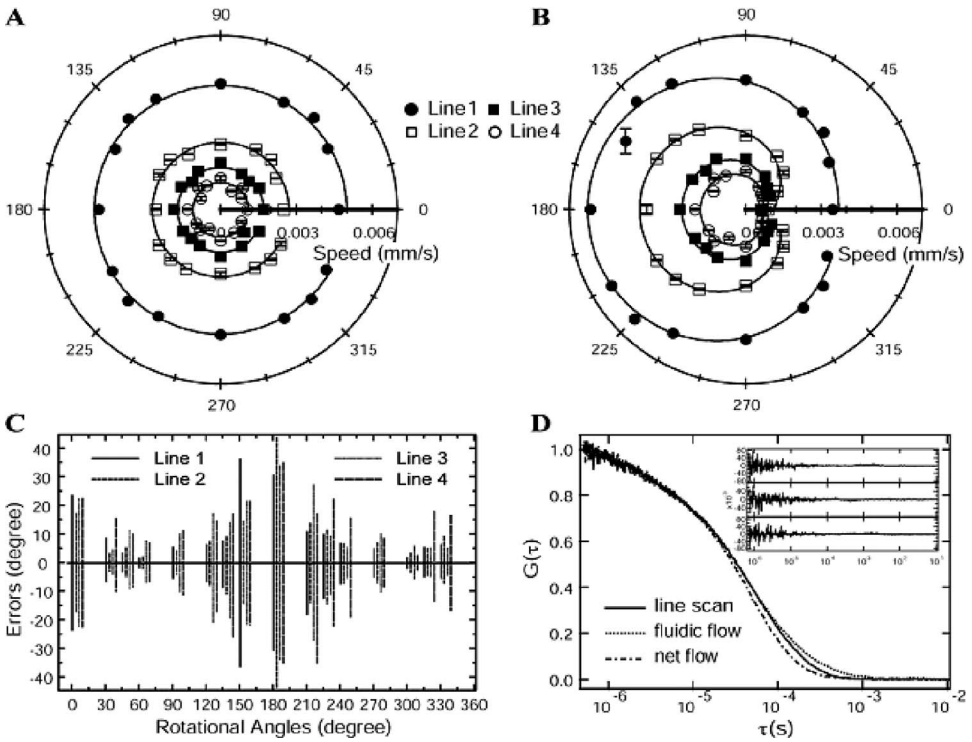

Fig. 5 Calibrations of flow direction analysis by slow line-scan FCS: (A) scanning speeds measured in a stationary sample and (B) net speeds measured with the pumping rate of 1 ml/h plotted at 16 rotation angles in the polar graphs for four different scan lines. The lengths of lines 1, 2, 3, and 4 are 3, 6, 12, and 25 μm, respectively. (C) Standard deviation of all measurements and (D) experimental ACF curves of line scan, microfluidic flow, and net flow shown with their respective fitting residues (inset, from top to bottom).

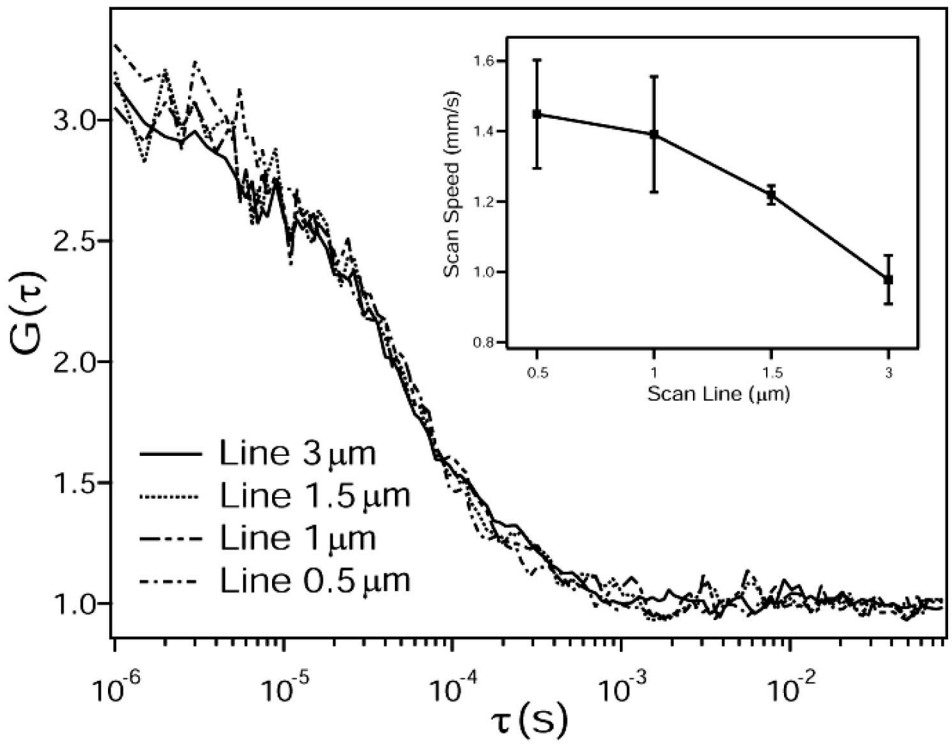

Fig. 6 ACF curves of four scan lines with decreasing lengths (3, 1.5, 1, and 0.5 μm) and the respective increasing line-scan speeds (inset). The length of a scan line was reduced by partial acquisition of fluorescence fluctuations in forward scans.

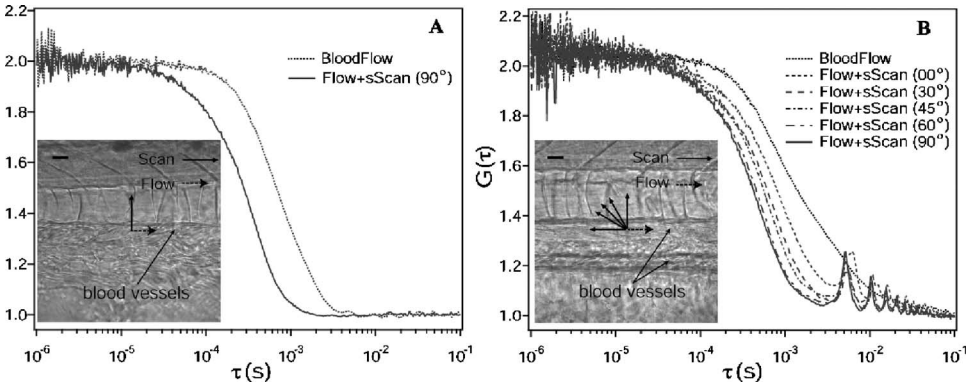

Fig. 7 Normalized ACF curves of zebrafish blood flow and net flow when coupled with line scans at various angles, where the respective vectors of scan and flow are shown in insets: (A) a blood flow angle of 12.6 deg was obtained by line scan FCS at 90 deg and (B) the interference of periodic line scan is shown as peaks in ACF curve for some special cases. The solid lines in the inset represent the effective scan vectors at different angles, from 0, 30, 45, 60, and 90 deg (clockwise).

flow profile. Velocity vectors were then calculated and superimposed onto an image of the microchannel [Fig. 3(B)], where the length of the vector represents flow speed and its arrow indicates flow direction. The resultant figure of the obstruction microfluid velocity profile is qualitatively consistent with that obtained[11] by PIV.

Another application of line-scan FCS is realized in small blood vessels of living zebrafish tissue. Potentially this is a label-free method since the autofluorescence of flowing proteins and red blood cells in zebrafish blood provides sufficient signal fluctuations for FCS measurements. Note that nanomolar concentrations of a fluorophore can be injected into zebrafish embryos in an early developmental stage[36] when no red blood cells exist to enable FCS measurements. This still has a strong advantage over PIV, since small concentrations of fluorophores are unlikely to block small vessels. In the experiments, the blood vessel of the immobilized zebrafish on the microscopic stage was aligned to be horizontal; the schematic vectors for blood flow and line scans are superimposed onto a transmitted image [Figs. 7(A) and 7(B)]. Single-point FCS and slow line-scan (90 deg) FCS were performed and all the data were fit with the two-flow model. A two-flow model must be used for adequate fitting since there are alternating slow and fast blood flows in the zebrafish cardiac cycle stemming from systolic and diastolic periods. In combination with the slow line scan, which can be treated as a single flow as shown earlier, this leads to two alternating flow patterns determined by the slow line scan overlaid with either the systolic or diastolic flow speed. The flow angle was calculated to 12.6 deg using Eq. (5) [Fig. 7(A)]. A problem arises for this method in cases where there are obstructions in the scanning path, as, for instance, a blood vessel wall. For this case, a periodic signal will be seen in the ACF and the fitting of the data is difficult or even impossible, especially if the obstruction should have a slow movement itself. However, the scanning period is in the range of milliseconds or more, hence, on the time scale it will not contribute to the width of the ACF curve of the diffusion plus flow. Therefore, by recording slow line scan FCS at different rotation angles (0, 30, 45, 60, and 90 deg) the blood flow direction can still be determined [Fig. 7(B)]. In this example, the ACF possesses its greatest width at a scan angle of 0 deg, indicating that the flow is horizontal, as expected. Scanning in multiple directions thus enables measurements of flow profiles even in small blood vessels and close to obstructions and vessel walls. In addition, this approach is independent of the focal dimensions, which can be strongly distorted in tissues. As a last point, note that the measured ACFs contain as well periodic fluctuations in the second time scale due to the heart rate of the organisms (data not shown). While this is not of interest in the flow profile measurements, it enables the accurate online monitoring of the heart beat frequency of the organism measured.

4.6 *Discussions*

The spatial resolution of line-scan FCS was limited by the length of scan lines, and was also affected by the inherent nonlinear behavior of scanning mirror mechanism at line endpoints. This problem could be solved as shown in Sec. 4.3 by using fluorescence signals collected during a specific phase of the line scan, although that reduces signal collection time and might increases the necessary measurement time. A critical drawback of the combined system lies in the fixed time ratios of forward and backward line scans, as fixed by the commercial FV300 system, which makes available a few line scan speeds. Optimized ratios, which minimize the deviation of the measurements from a one-flow model and have small nonlinearities at the scan endpoints, could be achieved by the direct control of the scanning mirrors. In that case, the spatial resolution of line-scan FCS for characterization of flow profiles might be improved further. The advantage of FCS over other methods is that only a low concentration ($\sim$1 nM) and small-size molecules is required, and thus clogging of channels and blood vessels as can happen with PIV is not a problem. This means as well that this technique can be used in nanoscale channels too small to allow PIV measurements with microbeads. Importantly, the method works for the measurements in blood vessels when autofluorescence is high enough. Asymmetric-focus FCS requires the distortion of the focal volume interfering with the imaging capabilities of the microscope and it is ambiguous since opposite flow directions cannot be resolved and are difficult be apply to tissue measurements. Dual-beam FCS requires the installation of an extra pinhole in the instrument. In contrast to these two techniques,

line-scan FCS can be implemented on any commercial or custom-built confocal microscope system based on a simple modification without interference in the imaging capabilities. In addition, by scanning the laser focus using a piezoactuator in the z direction, the presented method could be extended for measurements of 3-D microfluidic flow velocities. The combination system could thus enable 3-D flow to be locally measured in the context of structural features, which is important to easily correlate the flow environments with particular cells or tissue structures in small animal bodies. This feature also has a potential application in tissue engineering to optimize the fluidic culture system.

5 Conclusions

We performed line-scan FCS experiments on a modified laser scanning confocal microscope and demonstrated its applications in the analysis of flow profiles in microchannels and its feasibility of flow direction determination in living zebrafish blood vessels. The accuracy of line scan FCS was assessed in dependence of (1) the angle between scanning direction and flow, (2) the scan speed, and (3) the scan length used in the experiments. We chose a line scan length of 3 μm as a compromise between spatial resolution and measurement accuracy. With the current setup, the measurement errors can be as low as ±10 deg. The potential extension of the method for 3-D microfluidic flow velocities was also discussed. Hence, line-scan FCS is a good alternative for noninvasive, minimally disturbing flow profile analyses in many applications. The combination of imaging and spectroscopy tools also facilitates a precise positioning of measurement points inside a microstructure with complicated geometry, such as fluidic microchannels, cell-culture microstructures, and biological tissues, and thus line-scan FCS could be a very useful tool for the characterization of their flow profiles.

Acknowledgments

We acknowledge the technical assistance from other members of the Wohland and Yu laboratories and the infrastructure support from the National University Medical Institutes as well as the Institute of Bioengineering and Nanotechnology. This work is supported in part by grants from Ministry of Education, Biomedical Research Council and National Medical Research Council of Singapore. XP is a research scholar of the National University of Singapore.

References

1. B. H. Weigl, R. L. Bardell, and C. R. Cabrera, "Lab-on-a-chip for drug development," *Adv. Drug Delivery Rev.* **55**, 349–377 (2003).
2. P. S. Dittrich and P. Schwille, "An integrated microfluidic system for reaction, high-sensitivity detection, and sorting of fluorescent cells and particles," *Anal. Chem.* **75**, 5767–5774 (2003).
3. M. Foquet, J. Korlach, W. Zipfel, W. W. Webb, and H. G. Craighead, "DNA fragment sizing by single molecule detection in submicrometer-sized closed fluidic channels," *Anal. Chem.* **74**, 1415–1422 (2002).
4. M. U. Kopp, A. J. Mello, and A. Manz, "Chemical amplification: continuous-flow PCR on a chip," *Science* **280**, 1046–1048 (1998).
5. M. J. Powers, K. Domansky, M. R. Kaazempur-Mofrad, A. Kalezi, A. Capitano, A. Upadhyaya, P. Kurzawski, K. E. Wack, D. B. Stolz, R. Kamm, and L. G. Griffith, "A microfabricated array bioreactor for perfused 3D liver culture," *Biotechnol. Bioeng.* **78**, 257–269 (2002).
6. S. Kaihara, J. Borenstein, R. Koka, S. Lalan, E. R. Ochoa, M. Ravens, H. Pien, B. Cunningham, and J. P. Vacanti, "Silicon micromachining to tissue engineer branched vascular channels for liver fabrication," *Tissue Eng.* **6**, 105–117 (2000).
7. Y. C. Toh, S. Ng, Y. M. Khong, V. Samper, and H. Yu, "A configurable three-dimensional microenvironment in a microfluidic channel for primary hepatocyte culture," *Assay Drug Dev. Technol.* **3**, 169–176 (2005).
8. M. L. Smith, D. S. Long, E. R. Damiano, and K. Ley, "Near-wall micro-PIV reveals a hydrodynamically relevant endothelial surface layer in venules *in vivo*," *Biophys. J.* **85**, 637–645 (2003).
9. A. M. Rollins, S. Yazdanfar, J. K. Barton, and J. A. Izatt, "Real-time *in vivo* color Doppler optical coherence tomography," *J. Biomed. Opt.* **7**, 123–129 (2002).
10. E. Nagel, T. Thouet, C. Klein, S. Schalla, A. Bornstedt, B. Schnackenburg, J. Hug, E. Wellnhofer, and E. Fleck, "Noninvasive determination of coronary blood flow velocity with cardiovascular magnetic resonance in patients after stent deployment," *Circulation* **107**, 1738–1743 (2003).
11. J. G. Santiago, S. T. Wereley, C. D. Meinhart, D. J. Beebe, and R. J. Adrian, "A particle image velocimetry system for microfluidics," *Exp. Fluids* **25**, 316–319 (1998).
12. H. Cheng, Q. Luo, S. Zeng, S. Chen, J. Cen, and H. Gong, "Modified laser speckle imaging method with improved spatial resolution," *J. Biomed. Opt.* **8**, 559–564 (2003).
13. W. Wang, Y. Liu, G. J. Sonek, M. W. Berns, and R. A. Keller, "Optical trapping and fluorescence detection in laminar flow streams," *Appl. Phys. Lett.* **67**, 1057–1059 (1995).
14. B. Manz, P. Stilbs, B. Joensson, O. Soederman, and P. T. Callaghan, "NMR imaging of the time evolution of electroosmotic flow in a capillary," *J. Phys. Chem.* **99**, 11297–11301 (1995).
15. E. L. Elson and D. Magde, "Fluorescence correlation spectroscopy. I. Conceptual basis and theory," *Biopolymers* **13**, 1–27 (1974).
16. D. Magde, W. W. Webb, and E. L. Elson, "Fluorescence correlation spectroscopy. III. uniform translation and laminar flow," *Biopolymers* **17**, 361–376 (1978).
17. R. H. Kohler, P. Schwille, W. W. Webb, and M. R. Hanson, "Active protein transport through plastid tubules: velocity quantified by fluorescence correlation spectroscopy," *J. Cell. Sci.* **113**, 3921–3930 (2000).
18. B. H. Kunst, A. Schots, and A. J. Visser, "Detection of flowing fluorescent particles in a microcapillary using fluorescence correlation spectroscopy," *Anal. Chem.* **74**, 5350–5357 (2002).
19. M. Gosch, H. Blom, J. Holm, T. Heino, and R. Rigler, "Hydrodynamic flow profiling in microchannel structures by single molecule fluorescence correlation spectroscopy," *Anal. Chem.* **72**, 3260–3265 (2000).
20. K. K. Kuricheti, V. Buschmann, and K. D. Weston, "Application of fluorescence correlation spectroscopy for velocity imaging in microfluidic devices," *Appl. Spectrosc.* **58**, 1180–1186 (2004).
21. P. F. Lenne, D. Colombo, H. Giovannini, and H. Rigneault, "Flow profiles and directionality in microcapillaries measured by fluorescence correlation spectroscopy," *Single Mol.* **3**, 194–200 (2002).
22. M. Brinkmeier, K. Dorre, J. Stephan, and M. Eigen, "Two-beam cross-correlation: a method to characterize transport phenomena in micrometer-sized structures," *Anal. Chem.* **71**, 609–616 (1999).
23. K. Q. Xia and Y. B. Xin, "Dual-beam incoherent cross-correlation spectroscopy," *J. Opt. Soc. Am. A* **12**, 1571–1578 (1995).
24. P. S. Dittrich and P. Schwille, "Spatial two-photon fluorescence cross-correlation spectroscopy for controlling molecular transport in microfluidic structures," *Anal. Chem.* **74**, 4472–4479 (2002).
25. N. O. Petersen, "Scanning fluorescence correlation spectroscopy. I. Theory and simulation of aggregation measurements," *Biophys. J.* **49**, 809–815 (1986).
26. D. E. Koppel, F. Morgan, A. E. Cowan, and J. H. Carson, "Scanning concentration correlation spectroscopy using the confocal laser microscope," *Biophys. J.* **66**, 502–507 (1994).
27. K. M. Berland, P. T. So, Y. Chen, W. W. Mantulin, and E. Gratton, "Scanning two-photon fluctuation correlation spectroscopy: particle counting measurements for detection of molecular aggregation," *Biophys. J.* **71**, 410–420 (1996).
28. B. Hebert, S. Costantino, and P. W. Wiseman, "Spatiotemporal image correlation spectroscopy (STICS) theory, verification, and application to protein velocity mapping in living CHO cells," *Biophys. J.* **88**, 3601–3614 (2005).
29. J. P. Skinner, Y. Chen, and J. D. Muller, "Position-sensitive scanning fluorescence correlation spectroscopy," *Biophys. J.* **89**, 1288–1301

(2005).
30. R. Rigler, U. Mets, J. Widengren, and P. Kask, "Fluorescence correlation spectroscopy with high count rate and low background: analysis of translational diffusion," *Eur. Biophys. J.* **22**, 169–175 (1993).
31. J. Widengren, U. Mets, and R. Rigler, "Fluorescence correlation spectroscopy of triplet states in solution: a theoretical and experimental study," *J. Phys. Chem.* **99**, 13368–13379 (1995).
32. M. Westerfield, *The Zebrafish Book. A Guide for the Laboratory Use of Zebrafish (Danio rerio)*, 4th ed., Univ. of Oregon Press, Eugene (2000).
33. D. E. Koppel, "Statistical accuracy in fluorescence correlation spectroscopy," *Phys. Rev. A* **10**, 1938–1945 (1974).
34. T. Wohland, R. Rigler, and H. Vogel, "The standard deviation in fluorescence correlation spectroscopy," *Biophys. J.* **80**, 2987–2999 (2001).
35. U. Meseth, T. Wohland, R. Rigler, and H. Vogel, "Resolution of fluorescence correlation measurements," *Biophys. J.* **76**, 1619–1631 (1999).
36. S. Isogai, M. Horiguchi, and B. M. Weinstein, "The vascular anatomy of the developing zebrafish: an atlas of embryonic and early larval development," *Dev. Biol.* **230**, 278–301 (2001).